Crystal growth and composition-property relationship of $Ce_3Pd_{20}Si_6$ single crystals

A. Prokofiev,[1,*] J. Custers,[1] M. Kriegisch,[1] S. Laumann,[1] M. Müller,[1] H. Sassik,[1] R. Svagera,[1] M. Waas,[1] K. Neumaier,[2] A. M. Strydom,[3] and S. Paschen[1,†]

[1]*Institute of Solid State Physics, Vienna University of Technology, Wiedner Hauptstr. 8-10, 1040 Vienna, Austria*

[2]*Walther-Meißner-Institute for Low Temperature Research, Walther-Meißner-Str. 8, 85748 Garching, Germany*

[3]*Physics Department, University of Johannesburg, P.O. Box 524, Auckland Park 2006, South Africa*

(Received 12 March 2009; revised manuscript received 4 November 2009; published 3 December 2009)

To elucidate the discrepancies in low-temperature data reported on the quantum critical heavy fermion compound $Ce_3Pd_{20}Si_6$ and reveal the compound's intrinsic properties, single crystals of varying stoichiometry were grown by various techniques—from the melt and from high-temperature solutions using fluxes of various compositions. The resulting stoichiometry of the crystals as well as their physical properties show sizable dependence on the different growth techniques. The Ce content ΔCe varies by more than 3 at. % among all grown single crystals. We have revealed a systematic dependence of the residual resistance ratio, the lattice parameter, the (lower) phase-transition temperature T_L, and the maximum in the temperature dependent electrical resistivity T_{max} with ΔCe. This clarifies the sizable variation in the values of T_L reported in the literature. We discuss the physical origin of the observed composition-property relationship in terms of a Kondo lattice picture. We predict that a modest pressure can suppress T_L to zero and thus induce a quantum critical point.

DOI: 10.1103/PhysRevB.80.235107 PACS number(s): 71.20.Lp, 71.27.+a, 72.15.−v, 81.10.Dn

I. INTRODUCTION

The recent observation of magnetic field induced quantum criticality[1,2] in the cubic heavy fermion compound $Ce_3Pd_{20}Si_6$ (Ref. 3) has attracted considerable attention. $Ce_3Pd_{20}Si_6$ crystallizes in a cubic $Cr_{23}C_6$-type structure with the space group $Fm\bar{3}m$.[4] The cubic cell [a=12.161 Å,[4] 12.280 Å (Ref. 3)] contains 116 atoms. The Ce atoms occupy two distinct sites of cubic point symmetry. At the octahedral 4a (tetrahedral 8c) site Ce atoms are situated in cages formed by 12 Pd and six Si atoms (16 Pd atoms). These high coordination numbers allow to classify $Ce_3Pd_{20}Si_6$ as a cage compound. Strongly correlated cage compounds are of much interest as potential candidates for thermoelectric applications.[5]

In the isostructural germanide compound $Ce_3Pd_{20}Ge_6$ an antiferromagnetic (AF) and a quadrupolar (QP) phase transition have been found. These transitions were ascribed to two different Ce sublattices corresponding to the two crystallographic Ce sites.[6] Similar to the germanide compound, two phase transitions—a presumably antiferromagnetic one at T_L of 0.15,[3] 0.17,[7] or 0.31 K (Ref. 1) and a possibly quadrupolar one at T_U of 0.5 K (Ref. 1)—have been found in the silicide compound $Ce_3Pd_{20}Si_6$. Similar to the effect of magnetic field applied along [100] or [110] in $Ce_3Pd_{20}Ge_6$ (Ref. 8) magnetic field shifts the two transitions of polycrystalline $Ce_3Pd_{20}Si_6$ in opposite directions: At the critical field of about 1 T the transition at T_L is suppressed to zero whereas the transition at T_U shifts to 0.67 K.[1] The non-Fermi liquid behavior of the electrical resistivity, $\rho=\rho_0+AT$, observed at the critical field in the temperature range 0.1–0.6 K is an indication for the existence of a field-induced quantum critical point.[2]

Neutron scattering experiments on polycrystalline $Ce_3Pd_{20}Si_6$ have to date failed to detect any kind of magnetic order.[9] Thus, to clarify the nature of the phases below T_L and T_U large single crystals of high quality are needed. In fact, in the first neutron-scattering study on $Ce_3Pd_{20}Si_6$ single crystals[9] the absence of signatures of magnetic order was attributed to a too low T_L value of the investigated specimen.

Since both phase transitions take place at rather low temperatures, disorder may influence them significantly. The discrepancy in the reported ordering temperatures (e.g., Refs. 1, 3, and 7) demonstrates this delicate dependence. This has motivated us to undertake a systematic investigation of the relation between crystal-growth techniques/conditions, sample quality, and the resulting physical properties down to dilution refrigerator temperatures.

We show here that both phase transitions are extremely sensitive to small stoichiometry variations that result from different growth procedures. The corresponding sensitivity to lattice-parameter variations suggests that quantum criticality in $Ce_3Pd_{20}Si_6$ might be achieved by pressure—a notion which would make this compound especially well disposed toward a multiparameter study of this phenomenon.

II. EXPERIMENT

The polycrystalline starting material for crystal growth was synthesized by melting Ce, Pd, and Si in a horizontal water-cooled copper boat using HF heating. The purity of the starting materials was usually 99.99% for Ce (Ames Laboratory), 99.998% for Pd, and 99.9999% for Si, although lower purity metals (e.g., Pd 99.95%) were used for the first growth trials. Single crystal growth was performed by a variant of the floating zone melting technique using optical heating (Crystal Corporation four mirror furnace). All steps were done under Ar 6.0 protective atmosphere after several purgings with Ar.

The lattice parameters were determined by least-square refinements of X-ray diffraction spectra on powdered poly- and single crystalline samples using a Siemens D5000 diffractometer. Si was used as an internal standard.

Differential thermal analysis (DTA) was performed with a Linseis PT1750 in Ar 6.0 atmosphere and in alumina crucibles. The heating and cooling rates were 7 °C/min.

Polished cross-sections of the samples were investigated by scanning electron microscopy with energy dispersive x-ray analysis (SEM/EDX) using a Philips XL30 ESEM with an EDAX New XL-30 135–10 UTW+detector. All investigated samples were excited by 20 keV electrons.

To reduce the statistical error in the EDX measurements the amplifier time of the detector system was set to 10 μs, allowing for a reasonably high photon flux without significant loss of energy resolution. The overall integration time on a single sample was typically 3 to 5 h corresponding to total charges of 10–20 μC transferred to the sample. To avoid carbonaceous contamination of the sample surface due to too long exposure to the beam large sample areas of typically 10 μm$\times$10 μm were scanned, in most cases at several different positions of the sample.

Data reduction of the spectra and quantitative analysis were done by EDX Control Software (from EDAX Inc.) supplied by the manufacturer of the detector system. To improve the limited accuracy of the fundamental parameter approach employed by this program we used a polycrystalline $Ce_3Pd_{20}Si_6$ sample, the physical properties of which indicate high crystalline and stoichiometric perfection, as reference (see Sec. IV C). EDX measurements of all single crystals were accompanied by re-measuring this reference sample in order to eliminate the influence of eventual shifts of the instrument parameters (e.g., detector sensitivity function).

The typical sample size for electrical resistivity measurements was $3\times1\times0.5$ mm^3. For specific-heat measurements about 100 μm thin platelets with a mass of typically a few mg were used. All samples were cut with their smallest dimension in [100] direction which was roughly parallel (angle of about 15°) to the growth direction. Thus, any composition gradients due to possible segregation effects are minimal within each of the investigated samples.

The specific heat was measured with a relaxation-type method using a home-built setup in a ^{3}He/^{4}He dilution refrigerator. Electrical resistivity measurements were done by a standard four-point technique, with alternating dc current in a physical property measurement system from Quantum Design between room temperature and 2 K, and with low-frequency ac current in a ^{3}He/^{4}He dilution refrigerator from Oxford Instruments at temperatures below 2 K.

III. CRYSTAL GROWTH

A. Growth from the melt

To investigate the melting character of $Ce_3Pd_{20}Si_6$ a DTA run up to 1350 °C was carried out (Fig. 1). There is only a single peak both on the heating and on the cooling curve, indicating congruent melting as previously reported.[4] A closer inspection of the shape of the melting peak (Fig. 1, inset) might, however, suggest merely a quasicongruent melting character. The onset of melting occurs at $T_M \approx 1250$ °C. Because of undercooling the crystallization begins about 100 °C lower than the melting.

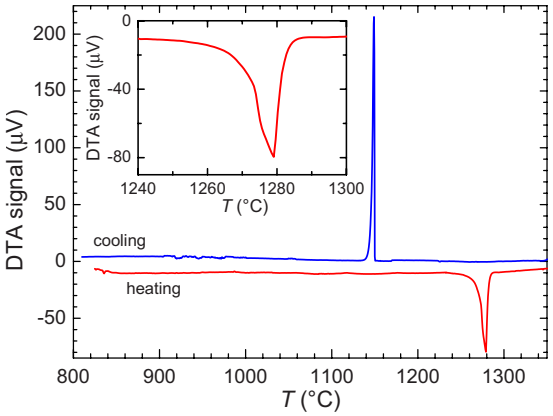

FIG. 1. (Color online) DTA curves of $Ce_3Pd_{20}Si_6$. The onset of melting at T_M is indicated. The inset shows a magnification of the melting peak.

The floating zone technique with optical heating was used for crystal growth from the melt, with a pulling rate of 10 mm per hour and an upper rod rotation speed of 5 rpm. Due to the high density and the low surface tension of the $Ce_3Pd_{20}Si_6$ melt the floating zone was rather unstable, and the melt dropped down repeatedly. However, one growth could be kept running long enough to grow an ingot of 25 mm length. Over the growth run the originally shiny and clear surface of the melt became more and more opaque, and a crust on the surface could be seen after some time. This is a sign of incongruent melting supposedly due to a peritectic reaction. The crust is the higher temperature phase, therefore it forms on the optically heated surface which is the hottest place of the melt. This observation can be explained by close proximity of the peritectic point to the temperature of the complete melting of the system with the total composition $Ce_3Pd_{20}Si_6$, as indicated already by the peculiar shape of the DTA curve (Fig. 1, inset). Therefore the formation of a small amount of foreign phase on the hot surface results in a slight shift of the melt composition, which returns the crystallization process in the melt deep into the primary crystallization field of the $Ce_3Pd_{20}Si_6$ phase.

Due to the thin foreign phase film the surface of the recrystallized (lower) rod was yellowish. The SEM/EDX measurement detected Ce (~70 at. %), Pd (~22 at. %), and Si (~8 at. %) in this film. However no inclusions of foreign phases were found by SEM/EDX inside the crystal. A single crystal grown in this way is specified here as *sc*1 (see Table I for the nomenclature of all crystals). In order to trace segregation effects we differentiate additionally between the part of this crystal grown at the beginning of the growth process (bottom part of the ingot, *sc*1*b*) and that grown at the end (top part, *sc*1*t*). For the growth of *sc*1 the lower purity starting materials (see Sec. II) were used.

Further growth runs with rotation of the upper rod led to a permanent breaking of the surface crust. The melt leaked out through the cracks of the crust. Hence, the crust may serve as a quasicrucible if it remains intact during the whole growth time. Based on this observation a growth run without rotation of the upper rod was carried out with the same growth parameters. The melt zone was quite stable in this experi-

TABLE I. Nomenclature of the $Ce_3Pd_{20}Si_6$ crystals grown by various techniques.

Sample name	Growth technique details
*sc*1*t*	From melt with rod rotation, top part
*sc*1*b*	From melt with rod rotation, bottom part
*sc*2	From melt without rod rotation
*sc*3	From Pd_5Si flux, molar $Ce_3Pd_{20}Si_6$ to Pd_5Si ratio 2:1
*sc*4	From Pd_5Si flux, molar $Ce_3Pd_{20}Si_6$ to Pd_5Si ratio 1:2
Sn flux crystals	Using Sn or Sn-Pd fluxes

ment. A crystal grown by this procedure will be specified as *sc*2. For the growth of this crystal higher purity starting materials (see Sec. II) were used.

Laue investigations show very good crystallographic perfection of both types of crystals grown from the melt. Before annealing an SEM/EDX investigation of both crystals was carried out. The polished cross-section of the *sc*1 rod is more homogeneous in composition than that of *sc*2. The surface of the latter had a well distinguishable 300 μm thick outer shell where the concentration of Ce was about 5% higher and that of Si somewhat lower than in the core region. This shell may result from a partial dissolution and diffusion of the crust into the core of the rod. In the core region of *sc*2 diffuse 10 μm inclusions of supposedly the same shell phase, however with lower Ce concentration, were found. These inclusions were not detected by x-ray powder diffraction and disappeared after annealing, according to SEM analysis.

After annealing of both crystals for 3 weeks at 900 °C a second EDX investigation was carried out. At first we did the analysis *without* any reference sample. This yielded a stoichiometric Ce content (10.3 at. %) but an over-stoichiometric Si content (22.0 instead of 20.7 at. %) and an under-stoichiometric Pd content (67.7 instead of 69.0 at. %) for both *sc*1 and *sc*2, corresponding to a partial substitution of Pd by Si on their sites. These results motivated our efforts to grow crystals using the flux technique, where the stoichiometry of the crystals can be tuned through the variation in the flux composition. The results of further EDX investigations *with* a reference sample will be discussed in Sec. IV C.

B. Flux growth

The reason for using the flux method was, on one hand, to obtain single crystals with exact stoichiometric composition and, on the other hand, the expectation that the off-stoichiometric melt would have a higher surface tension and hence that the floating zone would be more stable than without flux. To avoid a contamination by foreign atoms we first opted for self flux growth. Since the concentration of thermal defects (e.g., Si-Pd substitutions) in the crystal is expected to decrease with decreasing growth temperature, we searched for low-melting (at first binary) compounds/compositions with an over-stoichiometric Pd content.

TABLE II. Composition and lattice parameter *a* of the investigated $Ce_3Pd_{20}Si_6$ samples.

Sample name	Composition (at. %) Ce	Pd	Si	*a* (Å)
*sc*1*t*	10.5	67.6	21.9	12.276
*sc*1*b*	9.9	67.7	22.4	12.272
*sc*2	9.9	68.0	22.1	12.272
*sc*3	9.2	68.7	22.1	12.233
*sc*4	7.4	70.1	22.5	12.180
pc	10.1	67.7	22.2	12.280
Exact 3:20:6 stoichiometry	10.3	69.0	20.7	
Sn flux crystals	$CePd_{2-x}Si_{2+x}$			
Standard deviation	0.24	0.20	0.20	
Systematic error				<0.002

1. Pd_5Si *flux*

Pd_5Si fulfills all requirements: it melts at a relatively low temperature of 835 °C,[10] has an over-stoichiometric ($>20:6$) Pd/Si ratio, and there are no stable Ce-containing intermediate phases between Pd_5Si and $Ce_3Pd_{20}Si_6$ in the Ce-Pd-Si ternary phase diagram [cross-section at 600 °C (Refs. 11 and 12)].

As above, the floating zone technique with optical heating was used. The feed and the seed rods had the stoichiometric starting composition $Ce_3Pd_{20}Si_6$, and the zone was a molten mixture of $Ce_3Pd_{20}Si_6$ and Pd_5Si. Contrary to the melt growth, the floating zone was very stable, and its surface remained clear during the entire growth run. The latter means that the growth occurred within the $Ce_3Pd_{20}Si_6$ primary crystallization field. The stability of the melt zone allowed the rotation of the upper rod. Two growth runs with different flux compositions (molar ratios $Ce_3Pd_{20}Si_6$ to Pd_5Si of 2:1 and 1:2) were carried out. The crystals were annealed for 3 weeks at 900 °C. The corresponding samples are referred to as *sc*3 and *sc*4, respectively.

2. *Sn-based fluxes*

Since, as we show below, the self flux technique did not yield satisfying results we tested also foreign fluxes. The related compound $Ce_2Pd_3Si_5$ can be grown with Sn as flux at below 1100 °C.[13] To check for the compatibility of Sn flux with $Ce_3Pd_{20}Si_6$, a mixture of $Ce_3Pd_{20}Si_6$ and Sn was heated up to 1100 °C in a boron nitride crucible and then cooled slowly (1 °C/h) down to 700 °C. The solute-to-solvent ratio was 2:1. After crystallization the ingot was cut, polished, and investigated by SEM/EDX and XRD.

The crystallization yielded relatively large single crystals of the nonstoichiometric phase $CePd_{2-x}Si_{2+x}$ with $x \approx 0.25$ (Table II), incorporated in a matrix of Sn_4Pd. In addition, small inclusions of other phases were found. The experiment thus shows the inapplicability of Sn as a flux because its affinity to Pd leads to a destruction of the $Ce_3Pd_{20}Si_6$ phase.

However other Sn-based flux compositions with a lower affinity to Pd can be provided by the Sn-Pd binary phase

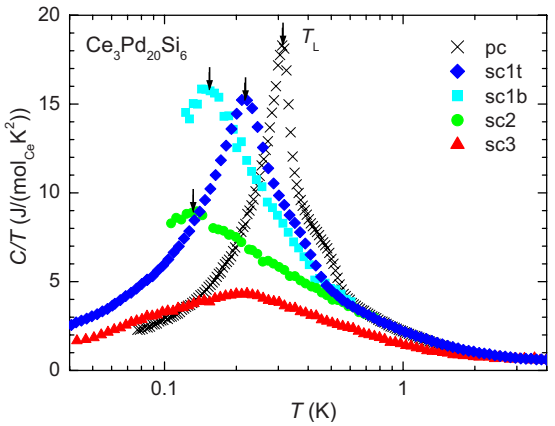

FIG. 2. (Color online) Specific heat divided by temperature C_p/T plotted for all single crystals prepared here, and for a polycrystal (Ref. 1) for comparison, as function of temperature T on a logarithmic scale. The lower transition temperatures T_L, taken here as position of the maxima are indicated by arrows. The maximum in the data for *sc*3 can be identified with T_U (see text).

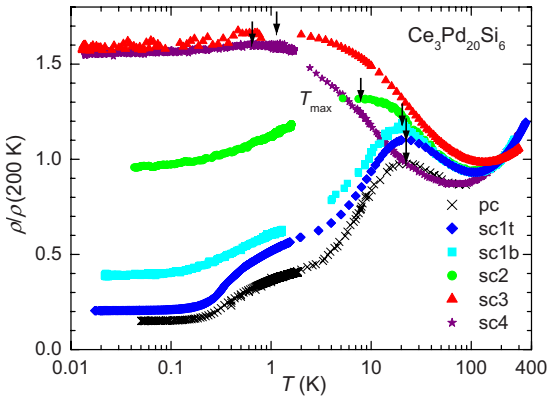

FIG. 3. (Color online) Electrical resistivity of all $Ce_3Pd_{20}Si_6$ single crystals grown here normalized to the respective 200 K values $\rho_{200\ K}$ vs temperature T. The arrows indicate the positions T_{max} of the (local) maxima. Data of a polycrystal (Ref. 1) are shown for comparison.

diagram.[10] A series of Sn-Pd compounds—Sn_4Pd, Sn_3Pd, Sn_2Pd—with low-melting points (below 600 °C) can be found there.

Similar experiments as the one with pure Sn flux were carried out using the above Sn-Pd compositions. In all cases according to SEM/EDX the primarily crystallized phase was $CePd_{2-x}Si_{2+x}$. The x value diminished with increasing Pd content in the flux, reaching about 0.05 for Sn_2Pd flux. The stoichiometric $CePd_2Si_2$ phase has the same Ce/Si ratio as the $Ce_3Pd_{20}Si_6$ phase but a strongly reduced Pd content. Further increasing of the Pd concentration in the flux was impossible: with the higher melting compound SnPd, only partial melting of the crucible content was observed at 1100 °C. Thus, foreign flux growth was not successful.

IV. PHYSICAL PROPERTIES

Neutron diffraction experiments were carried out on an oriented sample cut from *sc*1*b*. The crystal was confirmed to have excellent crystallinity but, contrary to our expectations from the investigations on polycrystalline samples, showed no phase transition down to the lowest accessed temperature of about 0.15 K.[9] The present investigation shows that, for this very single crystal, this temperature was still too high.

A. Specific heat

The specific heat C_p was measured for *sc*1−*sc*3. Figure 2 shows the temperature dependence of C_p/T of these crystals, together with published data of a polycrystalline sample.[1] $C_p/T(T)$ of the polycrystalline sample has a sharp peak with a maximum at T_L=0.31 K and a shoulder at $T_U \sim 0.5$ K.[1] These features get successively broadened and suppressed to lower temperatures in the crystals *sc*1*t*, *sc*1*b*, and *sc*2, respectively. In *sc*3 no clear signature of T_L can be identified, suggesting that it has shifted further to lower temperatures and was further broadened or, alternatively, has vanished altogether. Due to the suppression of this lower temperature feature the anomaly at T_U, identified in all other samples as shoulder, now appears as a maximum.

From specific heat the best single crystal thus appears to be *sc*1*t*. With its rather sharp peak at 0.22 K and a shoulder at about 0.4 K, it demonstrates all features associated with the intrinsic behavior of $Ce_3Pd_{20}Si_6$.

B. Electrical resistivity

The electrical resistivity of all single crystalline and of a polycrystalline sample is shown in Fig. 3 as function of temperature. While the resistivity of the polycrystalline sample drops to very low values at low temperatures, the residual resistivities of the single crystals are considerably higher. They increase in the sequence $pc \rightarrow sc1t \rightarrow sc1b \rightarrow sc2 \rightarrow sc3$. This is the same sequence in which the sharpness of the low-temperature phase transition of the C_p/T curves decreases (Fig. 2). Thus, it is natural to assume that in the sequence $pc \rightarrow sc1t \rightarrow sc1b \rightarrow sc2 \rightarrow sc3$ the lattice disorder increases. Since the starting material purity of *sc*1*t* and *sc*1*b* was lower than that of *sc*2, we conclude that the main reason of the disorder is a deviation of the sample composition from the exact stoichiometry 3:20:6 and not the concentration of foreign atoms. For single crystal *sc*4 the high-temperature minimum occurs at lower temperatures than expected, leading to a slightly lower residual resistivity than for *sc*3.

The highest residual resistance ratio [RRR, defined here as $\rho(200\ K)/\rho(50\ mK)$] and the sharpest and most pronounced phase-transition features in C_p/T are found for the polycrystalline sample (*pc*) which therefore appears to be the most stoichiometric. This can be easily understood by the specifics of preparation. The accuracy of the stoichiometric *total* composition of a polycrystalline sample is limited only by the accuracy of the weighing process of starting materials and by their purity. A possible high-temperature nonstoichiometry of the main phase of an as-cast polycrystal is compensated by the presence of minor impurity phases, the phase separation being heterogeneous on a microscopic scale. This heterogeneity can be lifted by annealing at lower temperatures due to the short diffusion path. During single-crystal

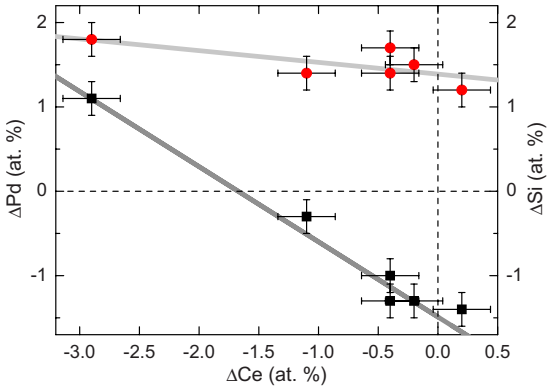

FIG. 4. (Color online) Deviation of the Pd and Si content, ΔPd and ΔSi, from the exact 3:20:6 stoichiometry as function of the Ce nonstoichiometry ΔCe. The dashed lines indicate the exact stoichiometry. The meaning of the broad gray lines is discussed in the text. Error bars indicate the standard deviations given in Table II.

growth, however, a macroscopic phase separation can occur, making annealing very inefficient. Actually the resistivity curves of *sc*1*b* before and after annealing were practically identical.

C. Composition of the grown crystals

Since the difference in the physical properties of the crystals is supposed to be caused by their varying stoichiometry much attention was paid to a more detailed investigation of the composition. The usual EDX technique without standards cannot determine absolute atomic concentrations with sufficient accuracy. This problem can, in principle, be solved by using a standard of exactly known composition. However, as such a sample is not readily available, we used, instead, the polycrystalline sample (*pc*) which was shown above to be of best quality. Irrespective of whether its composition may be identified with the *exact* stoichiometry 3:20:6 or not it served as a practical guideline to establish the crystal composition-property relationship.

With the additional improvements of our EDX technique (improved measurement statistics, counting time, beam current control, cf. Sec. II) we can measure, with a high accuracy, *deviations* from the reference sample stoichiometry. The results are summarized in Table II where the measured lattice parameters are given, too. Because crystals grown from the Sn-containing fluxes are not the title phase and their compositions vary sizably they are simply represented by $CePd_{2-x}Si_{2+x}$ in Table II.

Even though, in the absence of a standard, there remains some uncertainty about the *absolute* values measured by EDX (which even for the reference sample *pc* differ from the calculated stoichiometry 3:20:6), *trends* in the composition of the investigated series of crystals can be discussed. While the Si content varies only weakly a stronger variation of the Ce and Pd content is observed, the Ce concentration nearly anticorrelating with the one of Pd (Fig. 4).

V. DISCUSSION

While no clear correlation between the physical properties and the Si content can be demonstrated, a pronounced dependence on the Ce content (or anticorrelated Pd content) is observed (Fig. 4). Figure 5 shows the dependencies of the lattice parameter *a* and the RRR as function of the deviation from stoichiometry ΔCe. The largest deviations from the "intrinsic behavior" (which is most closely met by the polycrystal) are seen for *sc*4. It has the lowest Ce content of 7.4 at. % (ΔCe=2.9 at. %). The polycrystalline sample (*pc*) which demonstrates the most pronounced phase-transition features and *sc*1*t* with the second-sharpest features have the highest Ce contents, and the lowest deviation from the exact Ce stoichiometry. The deviation ΔCe of the latter (*sc*1*t*) lies on the other side of the stoichiometry line. One may argue that only the absolute value of ΔCe is relevant with respect to the composition-disorder-property relationship since *any* nonstoichiometry is usually associated with lattice imperfection. To test this conjecture we plot, in Fig. 5, the data point for *sc*1*t* also mirrored through the ΔCe=0 axis (open symbol). Indeed this point fits nicely into the overall RRR(ΔCe) behavior.

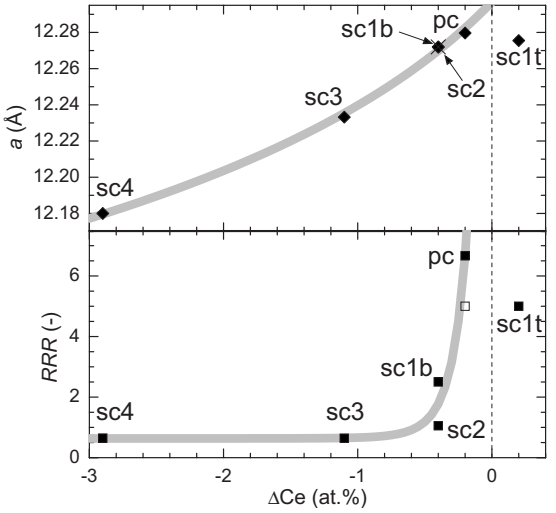

FIG. 5. Dependence of the lattice parameter *a* and the residual resistance ratio RRR on the deviation ΔCe from the stoichiometric Ce content. The open symbol in the lower panel represents the data point of *sc*1*t*, mirrored through the ΔCe=0 line. The thick gray lines are guides to the eye.

Ce *over*-stoichiometry can be realized by a substitution of Pd or Si atoms on their crystallographic sites by excess Ce atoms or, alternatively, by vacancies on the Pd and/or Si sites. Since the lattice parameter of *sc*1*t* is smaller than that of the *pc*, the latter option is more probable, but a combination of both options cannot be excluded. If only Pd/Si vacancies were present, the Ce sublattice would remain occupied and fully ordered. Ce *under*-stoichiometry, on the other hand, can be associated either with Ce vacancies or, which is more probable taking into account the approximate anticorrelation between the Ce and Pd contents, with a partial Pd substitution on Ce sites. The broad dark gray line in Fig. 4 represents the Ce-Pd concentration relation for a crystallochemical model which, as an example, assumes a half-filling of the Ce vacancies V^{Ce} by excess Pd atoms: $[Ce_{1-x}V^{Ce}_{0.5x}Pd_{0.5x}]Pd_{20}Si_6$. The same model was used to describe the ΔSi vs ΔCe relation (light gray line). The agreement with the data is excellent.

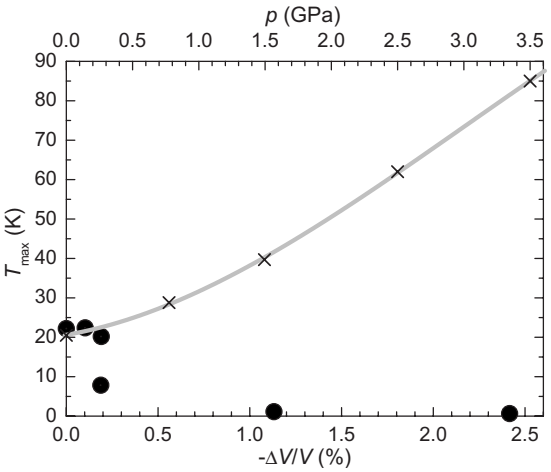

FIG. 6. Temperature T_{max} of the maximum in the electrical resistivity vs relative volume shrinkage $-\Delta V/V$ of our $Ce_3Pd_{20}Si_6$ single crystals with respect to the polycrystal (dots) and, for comparison, T_{max} vs pressure p for the polycrystal of Ref. 15 (crosses and gray line, which is a fit to the data). $\Delta V/V$ and p are related to each other via the bulk modulus of $Ce_3Pd_{20}Ge_6$ (Ref. 14).

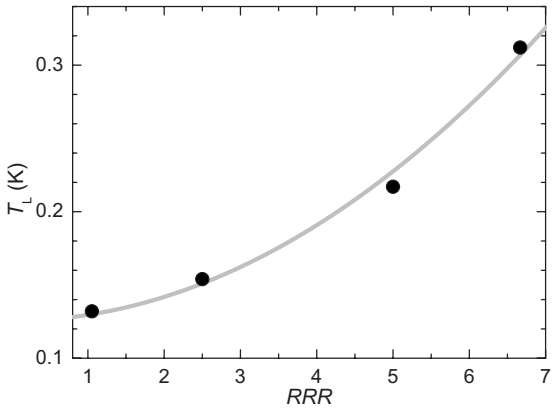

FIG. 7. Lower transition temperature T_L vs residual resistance ratio RRR for the different $Ce_3Pd_{20}Si_6$ samples. The line represents a quadratic fit to the data.

Both cases of Ce under-stoichiometry correspond, in a Kondo lattice description, to Kondo holes. In the Kondo coherent state at low temperatures Kondo holes act as strong scattering centers, decreasing the RRR. This effect is seen in the lower panel of Fig. 5. Since also *sc*1*t* has a reduced RRR, over-stoichiometry appears to be indeed realized by the combination of excess Ce and Pd/Si vacancies. Excess Ce, just as Ce holes, creates Kondo disorder. In addition to reducing RRR, Kondo disorder is expected to successively suppress the temperature T_{max} where the high-temperature incoherent Kondo scattering with an approximate $\rho \propto -\ln T$ behavior crosses over to coherent Kondo scattering at low temperatures. In samples *sc*3 and *sc*4 Kondo disorder is so strong that $\rho \propto -\ln T$ is observed in a wide temperature range and $\rho(T)$ shows only a tiny drop below 2 K. Figure 3 shows that a sizable suppression of T_{max} occurs in our sample series *pc*−*sc*1*t*−*sc*1*b*−*sc*2−*sc*3−*sc*4 only from *sc*2 on. Thus, in addition to Kondo disorder, there appears to be a second effect influencing T_{max} in the opposite direction. This can be identified as a volume effect: the Ce vacancies or (smaller) Pd atoms on Ce sites in Ce under-stoichiometric samples as well as the Pd or Si vacancies in the over-stoichiometric sample *sc*1*t* lead to a shrinkage of the crystal lattice, which is seen in Table II and the upper panel of Fig. 5. The decrease in volume with decreasing Ce content corresponds to positive (chemical) pressure. Using the bulk modulus of the closely related compound $Ce_3Pd_{20}Ge_6$ [~137.5 GPa at 150 K (Ref. 14)] we can convert the lattice shrinkage in our off-stoichiometric single crystals into a hypothetical external pressure p.

Figure 6 shows T_{max} (full dots) vs the relative volume shrinkage $-\Delta V/V$ of our single crystals with respect to our polycrystal (*pc*) (bottom axis) and vs a hypothetical external pressure calculated via the bulk modulus[14] (top axis). The steplike, as opposed to continuous, decrease in T_{max} with $-\Delta V/V$, addressed already above, is clearly seen. In order to understand this behavior we compare our results to a pressure study.[15] We include the T_{max} vs p data from this investigation on a polycrystalline sample under quasihydrostatic pressure in Fig. 6 (crosses and gray fit to these). From a value $T_{max} \approx 20$ K at $p=0$, similar to the value for our polycrystal, T_{max} increases continuously with increasing pressure. This behavior is typical for Ce-based heavy fermion compounds: With increasing pressure the hybridization between the 4*f* electron of Ce and the conduction electrons increases and thus the Kondo temperature which is proportional to T_{max} increases. Our data follow this trend only at low off-stoichiometry (low $-\Delta V/V$ values) while at higher off-stoichiometry T_{max} decreases quickly. Thus we conclude that the volume effect on T_{max} dominates in our sample series *pc*−*sc*1*t*−*sc*1*b*−*sc*2−*sc*3−*sc*4 up to *sc*1*b* while the Kondo disorder effect dominates from *sc*2 on.

Next we analyze the evolution of the ordering temperature T_L along our sample series. For this purpose T_L, extracted from the specific-heat data in Fig. 2, is plotted vs RRR in Fig. 7 and vs $-\Delta V/V$ (bottom axis) or p (top axis) in Fig. 8. T_L decreases continuously with decreasing RRR (Fig. 7). This might be taken as indication for the strong influence of disorder on T_L. However, in our sample series, the variation in RRR is intimately linked to a variation of ΔCe (Fig. 4) and thus to a variation in the lattice parameter a, the relative volume change $-\Delta V/V$, and the corresponding pressure p. Thus, an alternative view of the situation is that not increasing disorder but decreasing volume is responsible for suppressing T_L (Fig. 8). To decide which effect is dominant we come back to our above discussion on Fig. 6 which revealed that the volume effect on T_{max} dominates in the series *pc*−*sc*1*t*−*sc*1*b*−*sc*2−*sc*3−*sc*4 up to *sc*1*b* while the disorder effect dominates from *sc*2 on. If this holds true also for the effect on T_L it is Fig. 8 (without *sc*2) that captures the essential physics while Fig. 7 only displays implicit dependencies (except for *sc*2).

In a Kondo lattice picture the physical origin of the suppression of T_L with p is that pressure increases the hybridization between conduction electrons and 4*f* states, thus strengthening Kondo compensation, diminishing Ce magnetic moments, and suppressing the (most probably magnetic) ordering temperature T_L. Extrapolating the T_L vs p dependence of Fig. 8 to higher p suggests that a pressure

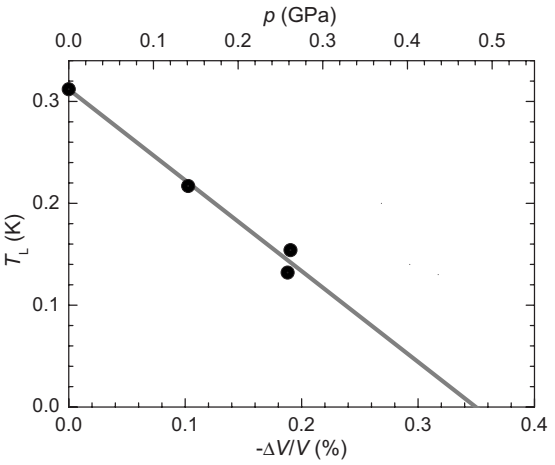

FIG. 8. Lower transition temperature T_L vs relative volume shrinkage $-\Delta V/V$ of the different $Ce_3Pd_{20}Si_6$ single crystals with respect to the volume of the polycrystal *pc*. On the upper axis the corresponding pressure as estimated via the bulk modulus of $Ce_3Pd_{20}Ge_6$ (Ref. 14) is given. The line represents a linear fit to the data and its extrapolation to $T_L=0$.

induced quantum critical point is at reach for $Ce_3Pd_{20}Si_6$. A linear extrapolation of the fit shown in Fig. 8 yields $p_c \approx 0.5$ GPa. Of course, actual low-temperature pressure measurements are needed to verify this possibility.

Finally, we comment on a related study on the germanide compound $Ce_3Pd_{20}Ge_6$ where the influence of the starting composition on the physical properties was investigated.[16] A strong composition effect on C_p and ρ was found to occur inside a narrow homogeneity range where a volume contraction of up to 0.7% takes place with increasing Pd content. In that work the concentration of Pd and not of Ce was concluded to be variable and responsible for the changing physical properties. It should be noted that the real composition of the resulting phases was not investigated. Thus, it is plausible that the increasing Pd content is accompanied by a decreasing Ce content. Under this assumption the composition effect on the properties of $Ce_3Pd_{20}Ge_6$ and $Ce_3Pd_{20}Si_6$ are indeed comparable.

VI. CONCLUSIONS

Single crystals of the $Ce_3Pd_{20}Si_6$ phase were grown from the melt under various growth conditions and from a high-temperature solution using Pd_5Si as a flux. $Ce_3Pd_{20}Si_6$ melts quasicongruently, i.e., the peritectic temperature is very close to the temperature of the complete melting. This fact follows from our DTA experiments and the observation of the melting zone during the growth process. The floating zone with stoichiometric composition was very unstable because of the low surface tension, which made the melt growth problematic. In contrast, the off-stoichiometric flux growth ran stably but resulted in nonstoichiometric single crystals.

While the Si content varies only slightly for different crystals, the Ce and Pd contents do so sizably, the decrease in Ce being partially compensated by an increase in Pd. The existence of a homogeneity range in $Ce_3Pd_{20}Si_6$ is the reason for the strong variation in the properties of single crystals grown by different techniques. The sharpness of the lower (presumably antiferromagnetic) phase transition, its transition temperature T_L, the residual resistivity, and the temperature T_{max} of the (local) maximum in $\rho(T)$ were shown to be measures of the crystal quality. Based on all these properties the upper part of the crystal grown from the stoichiometric melt (*sc*1*t*) with rod rotation can be ranked as having the highest perfection among all the grown single crystals. Its lattice parameter together with its composition indicate that the slight off-stoichiometry is not dominated by Ce on Pd sites but by Pd vacancies, which do not directly disturb the $4f$ lattice.

A comparison with published pressure data shows that the reduced lattice parameter of our single crystals with small off-stoichiometry acts essentially as external pressure, increasing the $4f$-conduction electron hybridization and the (single ion) Kondo temperature and decreasing the (presumably magnetic) phase transition at T_L. At higher off-stoichiometry effects due to Kondo disorder become important. $Ce_3Pd_{20}Si_6$ is thus a new cubic heavy fermion compound where tuning to a quantum critical point appears to be feasible by easily accessible magnetic fields *and* pressures. A comparison of the action of these two tuning parameters will be very instructive. Low-temperature pressure measurements on highly stoichiometric samples are needed to confirm our conjecture.

ACKNOWLEDGMENTS

We are grateful to G. Behr, P. Lejcek and J. Kopecek for experimental support and to V. Peter for preparative work. Financial support of the Austrian Science Foundation (Project No. P19458-N16), the European Research Council (Advanced Grant No. 227378), and of UNIINVEST 2004 is gratefully acknowledged. A.M.S. acknowledges research support from the Science Faculty under I. C. Burger, the URC of UJ, and the SA-NRF (Grant No. 2072956).

*prokofiev@ifp.tuwien.ac.at
†paschen@ifp.tuwien.ac.at

[1] A. M. Strydom, A. Pikul, F. Steglich, and S. Paschen, J. Phys.: Conf. Ser. **51**, 239 (2006).
[2] S. Paschen, M. Müller, J. Custers, M. Kriegisch, A. Prokofiev, G. Hilscher, W. Steiner, A. Pikul, F. Steglich, and A. M. Strydom, J. Magn. Magn. Mater. **316**, 90 (2007).
[3] N. Takeda, J. Kitagawa, and M. Ishikawa, J. Phys. Soc. Jpn. **64**, 387 (1995).
[4] A. V. Gribanov, Y. D. Seropegin, and O. J. Bodak, J. Alloys Compd. **204**, L9 (1994).
[5] S. Paschen, in *Thermoelectrics Handbook*, edited by D. M.

Rowe (CRC, Boca Raton, 2006), Chap. 15.
[6] J. Kitagawa, N. Takeda, and M. Ishikawa, Phys. Rev. B **53**, 5101 (1996).
[7] T. Goto, T. Watanabe, S. Tsuduku, H. Kobayashi, Y. Nemoto, T. Yanagisawa, M. Akatsu, G. Ano, O. Suzuki, N. Takeda, A. Dönni, and H. Kitazawa, J. Phys. Soc. Jpn. **78**, 024716 (2009).
[8] J. Kitagawa, N. Takeda, M. Ishikawa, T. Yoshida, A. Ishiguro, N. Kimura, and T. Komatsubara, Phys. Rev. B **57**, 7450 (1998).
[9] S. Paschen, S. Laumann, A. Prokofiev, A. M. Strydom, P. P. Deen, J. R. Stewart, K. Neumaier, A. Goukassov, and J.-M. Mignot, Physica B **403**, 1306 (2008).
[10] M. Chandrasekharaiah, in *Binary Alloy Phase Diagrams*, 2nd ed., edited by T. Massalski (William W. Scott, Jr, USA, 1990).
[11] Y. D. Seropegin, A. V. Gribanov, O. L. Kubarev, A. I. Tursina, and O. I. Bodak, J. Alloys Compd. **317-318**, 320 (2001).
[12] A. V. Gribanov, P. Rogl, and Y. D. Seropegin, in *Noble Metal Systems*, Landolt-Börnstein, New Series (Springer, Berlin, 2006), Vol. IV/11B, p. 340.
[13] N. Dung, Y. Haga, T. Matsuda, T. Yamada, A. Thamizhavel, Y. Okuda, T. Takeuchi, K. Sugiyama, M. Hagiwara, K. Kindo, R. Settai, and Y. Onuki, J. Phys. Soc. Jpn. **76**, 024702 (2007).
[14] Y. Nemoto, T. Yamaguchi, T. Horino, M. Akatsu, T. Yanagisawa, T. Goto, O. Suzuki, A. Dönni, and T. Komatsubara, Phys. Rev. B **68**, 184109 (2003).
[15] T. Hashiguchi, N. Takeda, J. Kitagawa, N. Wada, S. Takayanagi, M. Ishikawa, and N. Mori, J. Phys. Soc. Jpn. **69**, 667 (2000).
[16] J. Kitagawa, N. Takeda, F. Sakai, and M. Ishikawa, J. Phys. Soc. Jpn. **68**, 3413 (1999).